Measurement 46 (2013) 2661–2671

Contents lists available at SciVerse ScienceDirect

Measurement

journal homepage: www.elsevier.com/locate/measurement

A parametric study on design of a microrate-gyroscope with parametric resonance

Ali Pakniyat, Hassan Salarieh *

Center of Excellence in Design, Robotics and Automation, Department of Mechanical Engineering, PO Box 11155-9567, Tehran, Iran

ARTICLE INFO

Article history:
Received 7 May 2012
Received in revised form 3 October 2012
Accepted 20 March 2013
Available online 4 April 2013

Keywords:
MEMS gyroscope
Parametric resonance
Nonlinear Mathieu equation
Design

ABSTRACT

Parametric excitation for MEMS gyroscopes can provide resonance in both the drive and the sense modes, even with mismatched natural frequencies. In this paper, requirements for such a condition are studied by analyzing the effect of each factor on the steady state amplitudes of the two modes. To develop a general study, the governing equation of the gyroscope is scaled and non-dimensionalized. The resulting governing equation is in the form of a cubic Mathieu equation coupled to a Duffing equation. In the study of the scaled system, for a gyroscope with matched natural frequencies, three sets of optimum designs are obtained. Then, the robustness of parametric excitation for a gyroscope with mismatching modes is shown. As the results indicate, parametric excitation is able to provide high accuracy and robustness for MEMS gyroscopes.

1. Introduction

MEMS gyroscopes are widely used in many applications because of their incredible properties of being small, light, highly reliable, low power consuming and cheapness. These devices are so small that can be integrated with the electronic circuits required for their operation. These factors have widened the use of gyroscopes to many industries. For instance, in automotive applications they are used for vehicle stability control, navigation assists and roll-over detection. In addition, in electronic industries, gyroscopes are used in image stabilizers of cameras, hand-held GPSs, 3D input devices and virtual reality. MEMS Gyroscopes are also used in robotics for various control purposes.

Because in microscale, fabrication of rotating parts confronts many problems, almost all MEMS gyroscopes are vibratory-type. In vibrating gyroscopes, a part of the sensor is always vibrating in one direction called the *drive mode*. If there is an outside rotation rate, the resulting Coriolis force, which is two times the cross-product of the present velocity vector and the rotation vector ($2v \times \Omega$), induces vibrations in one or more directions called the *sense mode*(*s*). There are two approaches for measuring the unknown rotation rate from this phenomenon: open-loop and closed-loop [1]. The first approach, which is an open-loop method, is to measure the amplitude of vibration in the sense modes. The other technique is a closed-loop method that calculates the unknown rotation rate from the required control signal to counterbalance the vibrations in the sense modes and neutralize it. In most cases, the open-loop approach is utilized and so is in this paper.

Various designs for MEMS gyroscopes have been proposed and used such as *Lumped Mass*(*es*) [1–8], *Tuning Forks* [1,6], *Ring-Type* [1,6,9] and *Cantilever-Type* [10–14] gyroscopes. For instance, Fig. 1 shows the structure of a MEMS gyroscope consisting of a single lumped mass which is considered in this paper. As stated earlier, an actuation force produces vibrations in the drive mode: *x*-direction. If the frame of the gyroscope has a rotation rate Ω_z in the *z*-direction, the resulting Coriolis force induces vibrations in the sense mode: *y*-direction. In most vibrating gyroscopes, the actuation force is a simple harmonic

* Corresponding author. Tel.: +98 21 6616 5538; fax: +98 21 66000021.
E-mail addresses: pakniyat@cim.mcgill.ca (A. Pakniyat), salarieh@sharif.ir (H. Salarieh).

0263-2241/$ - see front matter © 2013 Elsevier Ltd. All rights reserved.
http://dx.doi.org/10.1016/j.measurement.2013.03.022

Nomenclature

Physical parameters

X	coordinate in the drive mode
y	coordinate in the sense mode
z	coordinate in 3rd dimension of the coordinate system
t	time
m	mass of the proof mass
c_x and c_y	damping in the x and y directions
k_{x1} and k_{y1}	linear terms of stiffness in the x and y directions
k_{x3} and k_{y3}	cubic terms of stiffness in the x and y directions
Ω_z	rotation rate of the frame of the gyroscope which is considered to be only in the z direction
F^a	the actuating force
r_1	linear parametric excitation coefficient
r_3	cubic parametric excitation coefficient
$V(t)$	actuation voltage
V_a	amplitude coefficient of the actuation voltage
x^d_{max} and y^d_{max}	the desired maximum amplitudes in the x and y directions
L	specific length

Scaled parameters

α_x and α_y	scaled damping in the x and y directions
β_1	linear parametric excitation factor
β_3	cubic parametric excitation factor
δ_{x1} and δ_{y1}	scaled linear stiffness in the x and y directions
δ_{x3} and δ_{y3}	scaled cubic stiffness in the x and y directions
γ	scaled rotation rate of the frame
τ	scaled time
$(.)'$	derivative with respect to the scaled time τ
u and v	scaled coordinates in the x and y directions
u_{max} and v_{max}	maximum amplitudes in the u and v directions obtained from simulation of the non-dimensional system

function. This excitation function has many benefits both in mathematical analysis and in physical operation of the sensor. However, one problem associated with harmonic excitation is that in order to have high amplitudes, specifically in the sense mode, the actuation frequency should coincide with the natural frequencies of both the drive and the sense modes [1–4,15]. Although applying the excitation frequency in a desired value is possible, it might not be feasible to meet near-resonance conditions in both modes since imperfections in fabrication process result in different natural frequencies in the drive and the sense modes, which in turn result in a low quality factor (Q) for the sensor [1].

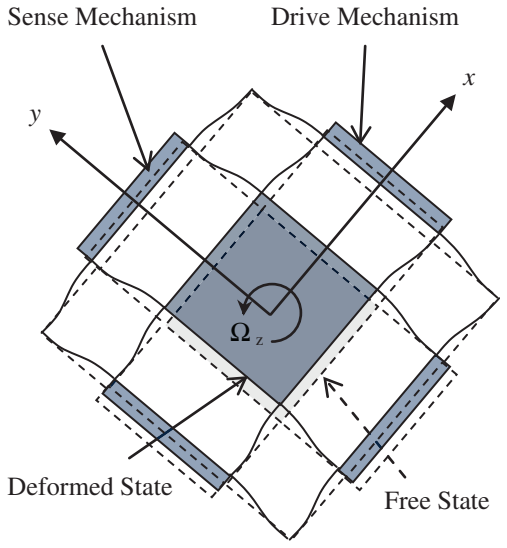

Fig. 1. Structure of the MEMS gyroscope considered in this paper.

To overcome the mentioned problem, a number of methods have been proposed and applied. These methods can be classified into three main categories. The first category employs some manufacturing tips and post-fabrication tunings. For instance Alper et al. [2–4] proposed a structure for providing a decoupled tunable spring structure and suggested some manufacturing tips such as adding an extra set of combs to tune the frequencies electrostatically. Also Liu et al. [16] matched the modes using improved spring beams by optimizing the shape of the suspension beams by a cellular automata approach. The second category is based on using some closed loop control techniques to match the modes. For example, one can refer to Batur et al. [5], Sung et al. [17,18] and Chang et al. [19]. These two approaches increase the cost of the sensor because of either extra manufacturing processes or additional electronics. However, the third category implements parametric resonance instead of harmonic resonance [15,20–22].

Parametric resonance has previously been implemented and utilized in various systems such as microbeams [23,24], mass sensors [25–30] and other systems. The benefit of parametric excitation is that resonance can be met even in frequencies far away from the natural

Table 1
The derivative operator and the scaling parameters.

$\alpha_x = \frac{2c_x}{m\omega}$	$\alpha_y = \frac{2c_y}{m\omega}$
$\beta_1 = \frac{2r_1V_A^2}{m\omega^2}$	$\beta_3 = \frac{2r_3V_A^2}{m\omega^2}$
$\delta_{x1} = \frac{4(k_{x1}+r_1V_A^2)}{m\omega^2} - \frac{\gamma^2}{4}$	$\delta_{y1} = \frac{4k_{y1}}{m\omega^2} - \frac{\gamma^2}{4}$
$\delta_{x3} = \frac{4(k_{x3}+r_3V_A^2)}{m\omega^2}$	$\delta_{y3} = \frac{4k_{y3}}{m\omega^2}$
$\gamma = \frac{4\Omega_z}{\omega}$	$2\tau = \omega t$
$(.)' = \frac{d(.)}{d\tau}$	

frequency of the system. The idea of employing parametric resonance for MEMS gyroscopes was first proposed by Oropeza-Ramos et al. [15,20–22]. However, as shown in this paper, the previously proposed design does not meet full resonance conditions and there exist much higher amplitude resonance orbits (around 1000 times larger) with better dynamic responses for such a device (around 10 times faster and with no overshoot in the transient response).

In this paper, in order to find the most desirable performance of the gyroscope, the effect of each factor on the response of the sensor is studied. Since there are too many parameter values to be selected (see Eq. (4) and Table 1), the number of design values is reduced using the design considerations in Section 3. Then in Section 4, the effect of each parameter on the output amplitude is studied and the optimal sets of parameter values are determined. The study shows that there are distinct regions in which the amplitude in the sense mode is significantly amplified due to resonance. For the range studied in this paper, three sets of such regions are determined and presented in Section 4.

2. Governing equations

The structure of the gyroscope considered in this paper is illustrated in Fig. 1 both in its unforced position (dashed lines) and its deflected state (solid lines). The structure of the suspension system is selected as shown in the figure in order to provide decoupled stiffness in the two directions [2–4]. According to the general governing equation derived in Appendix A, Eq. (1) shows the governing equation for the gyroscope based on the following assumptions:

a. The frame has negligible acceleration.
b. The frame's rotation rate is constant and is only in the z direction.
c. Motion in the z direction is restricted by comparatively higher stiffness resulting in $z = \dot{z} = \ddot{z} = 0$.
d. Dissipation is considered to behave as viscous damping (linear behavior).
e. Cross-coupling stiffness and damping are negligible.
f. The restoring force (stiffness) is considered to act cubically as $F_x^r(x) = k_{x1}x + k_{x3}x^3$ and $F_y^r(y) = k_{y1}y + k_{y3}y^3$.

$$\begin{cases} m\ddot{x} + c_x\dot{x} + k_{x1}x + k_{x3}x^3 = F^a + 2m\Omega_z\dot{y} + mx\Omega_z^2 \\ m\ddot{y} + c_y\dot{y} + k_{y1}y + k_{y3}y^3 = -2m\Omega_z\dot{x} + my\Omega_z^2 \end{cases} \quad (1)$$

Eq. (1) is the general Equation of motion for the considered MEMS gyroscope. As stated earlier, the actuation force F^a is the key factor in the operation of the sensor since it provides vibrations in the drive mode. Note that the exciting force in the sense direction is the Coriolis force $-2m\Omega_z\dot{x}$. Thus, in order to meet resonance conditions and hence, to have high amplitudes in the sense mode, this force should possess a large magnitude and a spectrum containing frequencies near the sense mode's natural frequency. Note that the only time-varying term in the Coriolis force in the sense mode is $\dot{x}$. Consequently, x should meet the mentioned conditions (the frequency content should be near the sense mode's natural frequency), which in turn requires the same conditions in the drive mode. In other words, the actuating force must provide resonance in the drive mode and this resonance response is required to contain mostly the frequency required to resonate the sense mode. This is the idea behind resonance-based MEMS gyroscopes.

If harmonic excitation is used, the natural frequency of the drive mode and the sense mode should be the same or at least very close to each other. However, in microfabrication, there are always unavoidable asymmetries that result in mismatched natural frequencies [1]. As a result, if one is interested in fabricating a resonance-based highly sensitive gyroscope, they are required to take some extra actions like post-fabrication tunings or closed loop control techniques. In Section 1, a brief review of these methods was presented.

In contrast, if parametric excitation is used for the actuation mechanism, resonance can be provided in both the drive and the sense modes. This is because of the fact that for parametric excitation, resonance in the drive mode occurs even with actuating frequencies far from the natural frequency. As a consequence, parametric resonance does not necessarily require matched modes and it is robust to mode mismatching. Implementing this idea for MEMS gyroscopes was first proposed by Oropeza-Ramos et al. [15,20–22]. As they suggested, an actuation function in the form of Eq. (2) and an actuating voltage in the form of Eq. (3) meet the desired goal.

$$F^a(x,t) = -(r_1x + r_3x^3)[V(t)]^2 \quad (2)$$

$$V(t) = V_A\sqrt{1+\cos\omega t} \quad (3)$$

Substituting Eqs. (2) and (3) in Eq. (1) and using the scaling parameters presented in Table 1, the scaled equation of motion can be presented as in

$$\begin{cases} x'' + \alpha_x x' + (\delta_{x1} + 2\beta_1\cos 2\tau)x + (\delta_{x3} + 2\beta_3\cos 2\tau)x^3 - \gamma y' = 0 \\ y'' + \alpha_y y' + \delta_{y1}y + \delta_{y3}y^3 + \gamma x' = 0 \end{cases} \quad (4)$$

The scaled equation of motion (Eq. (4)) is in the form of a Cubic Mathieu Equation coupled to a Duffing Equation. In order to obtain parametric resonance in the sensor, Oropeza-Ramos et al. [15,20–22] determined the required excitation parameter values based on a frequency response analysis on an existing gyroscope. However, a parametric study on design of the gyroscope [31] indicates that this method would not necessarily result in the highest possible amplitudes for the sensor. In this paper, a systematic method to find the maximum output amplitudes for the considered gyroscope is presented. For this purpose, the scaled governing equation (Eq. (4)) is considered and the effect of each parameter value on the output amplitude is studied. There are 10 scaled parameters whose values influence the system response. Among these 10, the scaled rotation rate (γ) is the input to the system and the other 9 are design parameters. In order to decrease the number of design parameters, we assume the design considerations in

Section 3. This way, there remain only 5 parameter values which can significantly influence the dynamic response. In Section 4, the effect of these values on the output amplitude is studied and the optimal values for them are indicated.

3. Design considerations

As discussed earlier, parametric resonance for a MEMS gyroscope does not necessarily require matched frequencies and it is robust to mode mismatching. So in general, different values can be considered for the stiffness in each direction, and based on the values selected, different sets of resonating parameters are found; while the gyroscope is still robust to differences in the stiffness values. In this paper, design procedure is based on equal natural frequencies and the robustness of this design to mismatching is studied. This means that the system is considered to have equal stiffness in both the drive and the sense modes ($k_{x1} = k_{y1}$ and $k_{x3} = k_{y3}$). Thus form Table 1, we can write

$$\begin{cases} \delta_{x1} = \delta_{y1} + 2\beta_1 \\ \delta_{x3} = \delta_{y3} + 2\beta_3 \end{cases} \tag{5}$$

Since the damping for this device is significantly due to the ambient pressure, damping is also considered to be the same in these two modes, i.e. $\alpha_x = \alpha_y = \alpha$. However, the procedure is not changed if different damping in the two modes is considered. As will be discussed later (see Section 4 and Fig. 5), the damping value has negligible effect on the steady state signal in the drive mode and it just determines the time required for dissipation of the transient response. However, damping has a great effect on the amplitude of the response in the sense mode (see Fig. 6). In our design procedure, we consider the reasonable value of 0.01 for the scaled damping α which provides high amplitude in the sense mode and a good time constant for the whole system. Note that since it is a design problem, in addition to changing the damping coefficient (c) by controlling the ambient pressure (which is common in fabrication of gyroscopes), the values of mass (m) and the excitation frequency (ω) can also be selected such that the scaled damping (α) from Table 1 meets the desired value.

The scaled rotation rate (γ) is the coupling term between the drive and the sense modes and hence, it might be desirable that γ be large. However, from Table 1 we see that during operation, a large γ changes the scaled stiffness in both the drive and the sense modes. As a matter of fact, a large γ moves the working conditions of the system away from resonance and results in a remarkable loss in the sensitivity of the gyroscope. Note that γ is not directly a design parameter, and only its range can be determined by the designer based on the desired readings of the sensor. As will be discussed later (see Section 4 and Fig. 3), a small change in a resonant δ_{y1} value contributes to a remarkable loss in the output amplitude of the gyroscope. As a conclusion, γ should be small, such as in the order of magnitude of 10^{-2} to 10^{-3}, so that while operating, γ^2 would not be able to change δ_{y1} from its desired value. In the design procedure, we consider the nominal value of 10^{-3} for γ and then show the output of the designed gyroscope for different values of γ (see Section 4 and Fig. 7).

In order to perform a non-dimensional analysis on the system, we define the specific-length L and scale all the lengths with respect to it. The non-dimensional equation for the gyroscope is presented in Eq. (6) where $u \triangleq x/L$ and $v \triangleq y/L$ so $x = L\,u$ and $v = L\,y$.

$$\begin{cases} u'' + \alpha u' + (\delta_{x1} + 2\beta_1 \cos 2\tau)u + (L^2\delta_{x3} + 2L^2\beta_3 \cos 2\tau)u^3 - \gamma v' = 0 \\ v'' + \alpha v' + \delta_{y1} v + L^2\delta_{y3} v^3 + \gamma u' = 0 \end{cases} \tag{6}$$

From Eq. (6) it can be concluded that the only terms that have a scaling effect on the amplitudes of the sensor are the terms containing L i.e. the nonlinear terms $L^2\delta_{x3}$, $L^2\delta_{y3}$ and $L^2\beta_3$ which are only two independent factors since $\delta_{x3} = \delta_{y3} + 2\beta_3$ holds. Using the non-dimensional equation of motion, the output of the gyroscope for $L^2\delta_{y3} = 1$ is determined and then, based on the required working dimensions of the sensor, L is chosen using Eq. (7) in which $x^d_{\max}$ and $y^d_{\max}$ are the desired amplitudes in the drive and the sense modes correspondingly and $u_{\max}$ and $v_{\max}$ are the maximum amplitudes obtained from simulation of the non-dimensional system.

$$L = \frac{x^d_{\max}}{u_{\max}} \text{ or } \frac{y^d_{\max}}{v_{\max}} \tag{7}$$

After this step, the required δ_{x3}, δ_{y3} and β_3 for the desired amplitudes of gyroscope are determined. Note that the term $L^2\beta_3$ has a destabilizing effect on the output of the gyroscope. A thorough study on the effect of this term is beyond the scope of this paper. It is just mentioned that since the time-varying term $2L^2\beta_3 \cos 2\tau$ changes the stiffness especially in large values of u, it weakens the stability of the steady state output of the sensor. In the present study, we initially consider a zero nominal value for β_3 (Fig. 2) and then we study its effect on the output of the gyroscope (Fig. 4). Note that when $\beta_3 = 0$, the equality $\delta_{x3} = \delta_{y3}$ holds.

4. Parameter values selection

As mentioned earlier, amplitude of the vibrations in the sense mode is used to measure the unknown rotation rate imposed to the gyroscope. Hence, in order to have more accurate readings, it is desired to make the amplitude in the sense mode as large as possible. In this section, through a parametric study of the sensor, the values of the scaled parameters are selected so that the maximum amplitude is achieved in the sense mode. Once these scaled parameters are selected, the physical parameters can be designed so that their corresponding scaled parameters satisfy the values found in this section. Note from Table 1 that the number of physical parameter values to be selected exceeds the number of scaled parameters by 4. Hence, the results found in this section can be brought back to their corresponding physical parameters in many ways, and for that, one is free to take other design considerations.

By considering $\alpha = 0.01$, $\beta_3 = 0$ and $L^2\delta_{y3}$ ($=L^2\delta_{x3}$) $= 1$ as discussed in Section 3, the maximum steady state

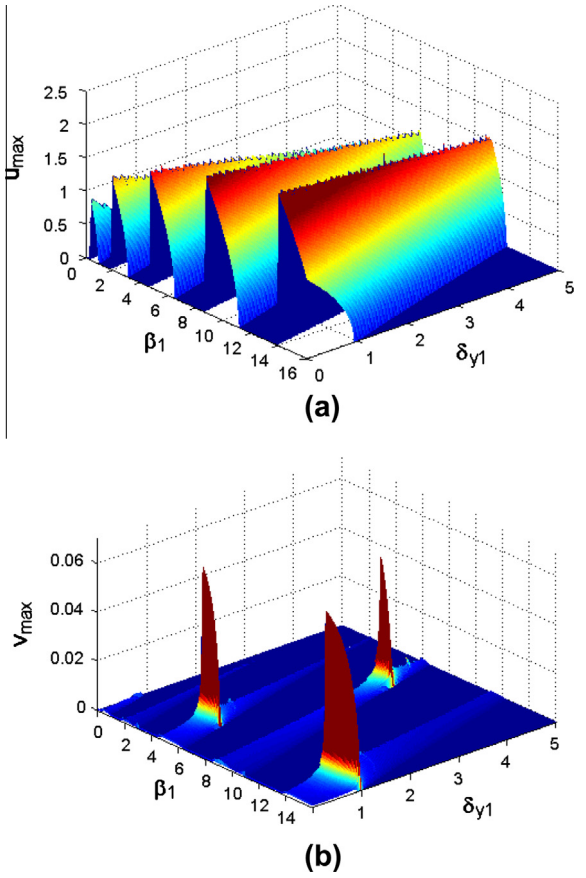

Fig. 2. Maximum non-dimensional steady state amplitude in (a) drive mode and (b) sense mode for different values of δ_{y1} and β_1.

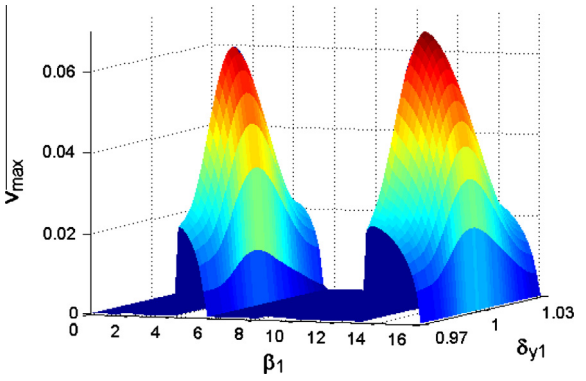

Fig. 3. Maximum non-dimensional steady state amplitude in sense mode near $\delta_{y1} = 1$.

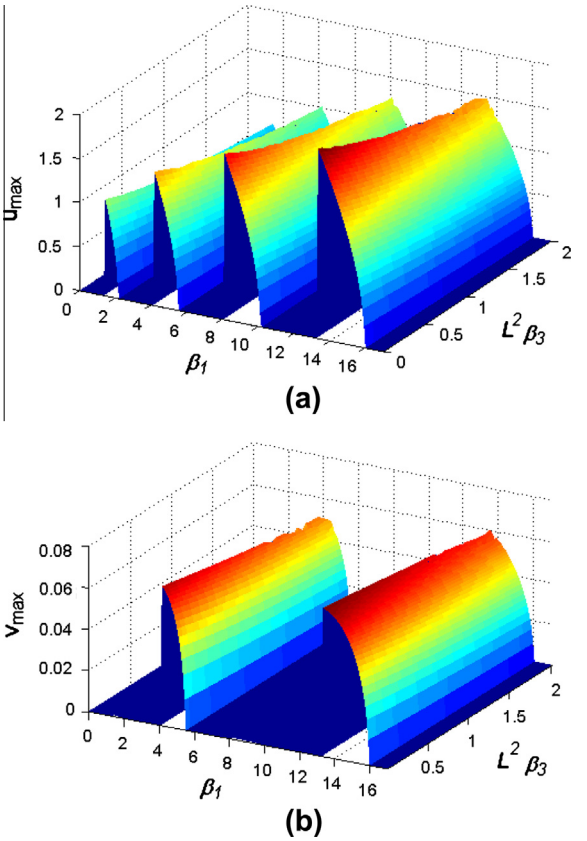

Fig. 4. Maximum non-dimensional steady state amplitude in (a) drive mode and (b) sense mode for different values of β_1 and $L^2\beta_3$.

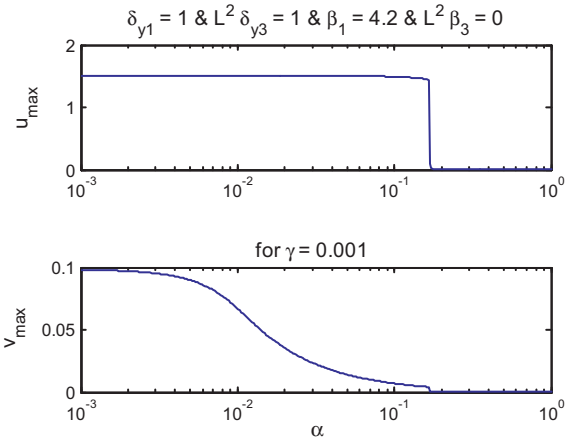

Fig. 5. Maximum Non-Dimensional Steady State Amplitude in Drive Mode (top) and Sense Mode (bottom) for different values of α.

amplitudes in both the drive and the sense modes for different values of δ_{y1} and β_1 are shown in Fig. 2.

Fig. 2 shows that even though the resonance regions in the drive mode are present for any value of δ_{y1}, only for few numbers of δ_{y1} (in Fig. 2, only for δ_{y1} near 1 and 4) the vibration produced in the drive mode contains the required frequency to provide resonance in the sense mode. This figure also suggests that the value of δ_{y1} is much more important for the sense mode rather than for the drive mode. A closer look at Fig. 2b near $\delta_{y1} = 1$ (Fig. 3) shows how a small change in δ_{y1} results in a dramatic loss in the sensitivity of the sensor. Therefore, the most important and critical parameter value that should

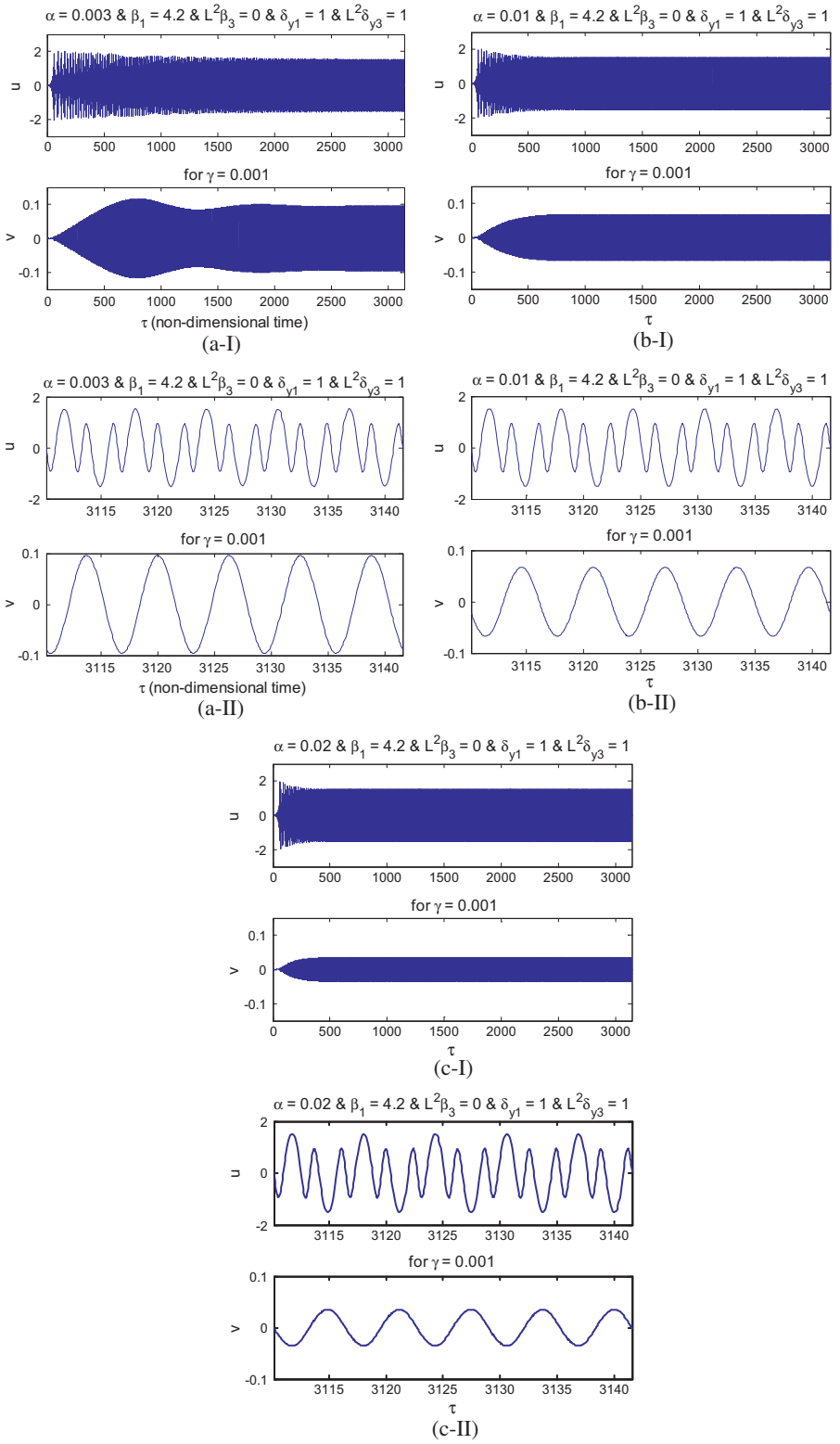

Fig. 6. Transient (I) and steady state (II) time responses of the system in drive mode (top) and sense mode (bottom) for (a) $\alpha = 0.003$, (b) $\alpha = 0.01$, (c) $\alpha = 0.02$.

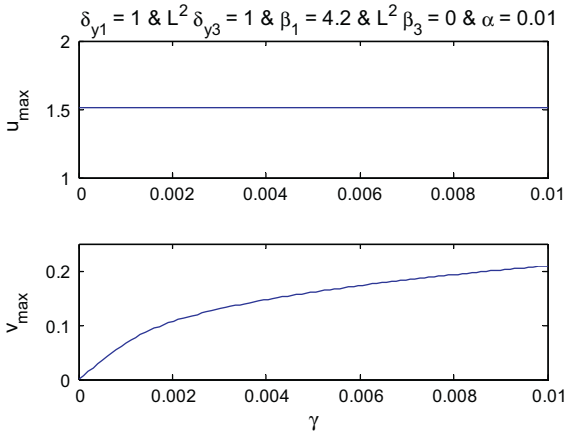

Fig. 7. Maximum non-dimensional steady state amplitude in drive mode (top) and sense mode (bottom) for different values of γ.

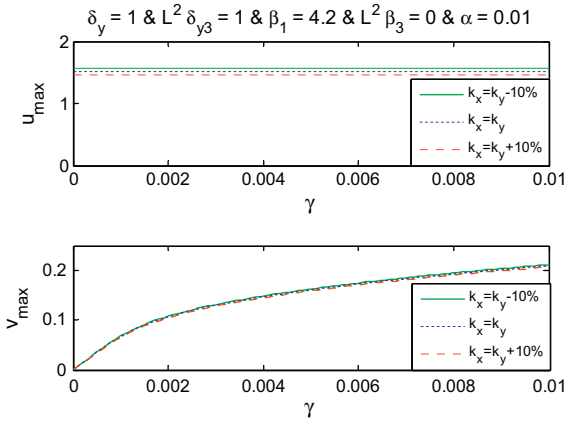

Fig. 8. Maximum non-dimensional steady state amplitude in drive mode (top) and sense mode (bottom) for different values of γ in presence of a 10% mismatching.

Table 2
The optimum regions for the scaled parameters of the system.

	Set 1	Set 2	Set 3	Considerations
δ_{y1}	1	1	4	Precise control on this value is required
β_1	4.1–5	13.3–15	6.4–7	See Figs. 2 and 3
β_3	0	0	0	Or as small as possible
i	0.01	0.01	0.01	Or some other value near this
γ	0–10^{-2}	0–10^{-2}	0–10^{-2}	Should be kept small, not to change δ_y

be kept constant would be δ_{y1}. This is feasible because γ is too small to change δ_{y1} significantly[1] and besides, actuation frequency can easily be tuned to provide such a condition.

[1] When γ is at most 10^{-3} to 10^{-2}, it is just able to change δ_{y1} less than 0.25×10^{-6} to 0.25×10^{-4}.

The effect of $L^2\beta_3$ in resonance corresponding to $\delta_{y1} = 1$ is shown in Fig. 4. For $\delta_{y1} = 4$ the behavior is similar. Fig. 4 shows that increasing $L^2\beta_3$ decreases the amplitude in both modes. In addition, as stated before, the third-order parametric excitation factor ($L^2\beta_3$) reduces the stability of periodic orbits. This means that $L^2\beta_3$ should be kept as close to zero as possible, i.e. the parametric excitation should be linear in the working dimensions of the gyroscope defined by the maximum amplitude for u. In physical terms, if non-interdigitated comb fingers are employed to provide parametric excitation (for example see [15]), increasing the number of such fingers decreases the nonlinearity of the excitation force.

To study the effect of α, we consider the values of $\delta_{y1} = 1$, $L^2\delta_{y3} = 1$, $\beta_1 = 4.2$ and $L^2\beta_3 = 0$ which are determined from the above results. For these values, the maximum steady state amplitude for different values of α ranging from 10^{-3} to 1 is shown in Fig. 5.

As Fig. 5 shows, the amplitude in the drive mode does not depend on α and the periodic response of the gyroscope is stable up to $\alpha \approx 0.17$, but for α greater than that, the periodic response becomes unstable and the origin becomes stable. As a result, α should be kept below this value.

The stability of the periodic response of the sensor is also influenced when α is far below 10^{-3}. A full study on the effect of α on the stability of periodic orbits is beyond the scope of this paper. It is just mentioned that by decreasing α, the ability of the system to fade disturbances is reduced and therefore, the periodic response of the sensor becomes unstable. For these values of α, the instability of the periodic response occurs while the origin is also unstable. Consequently, the system cannot reach a steady periodic solution. As a conclusion, the value of α should be kept between 10^{-3} and 10^{-1}.

From Fig. 5, it might seem that keeping $\alpha \approx 10^{-3}$ would be better than our previous choice $\alpha = 10^{-2}$, but as Fig. 6 (a, b, c) shows, even for $\alpha = 0.003$ the response is too slow and reaches its periodic orbit after about 1000 excitation cycles (equivalent to $\tau = 3142$). For $\alpha = 0.01$ this time is about 250 cycles and for $\alpha = 0.02$ is about 150 cycles which are comparatively small. Hence, for these values of α the steady response is fast enough because ω is usually in the order of 10^4 to 10^5 and the response time is related to τ by the relation $t = 2\tau/\omega$ (see Table 1). As stated before, the considered value $\alpha = 0.01$ results in both a high amplitude in the sense mode and a fast response in both modes.

The effect of the scaled rotation rate γ, which is the parameter the gyroscope is going to measure, is shown in Fig. 7. Since the coupling term γ is small, it has no significant effect on the amplitude of the drive mode. The effect of γ on the amplitude in the sense mode shown in the bottom of Fig. 7 is the calibration curve for the sensor.

To examine the robustness of this design, we consider a mismatching between the two modes. Note that although all the factors m, k_x, k_y and ω influence δ_{y1} and δ_{x1}, this mode mismatching can be supposed to be only due to difference in stiffness of the drive and the sense mode, because excitation frequency ω is always considered to be tuned in order to keep $\delta_{y1} = 1$. Fig. 8 shows the change in the output amplitude of the sensor due to a 10%

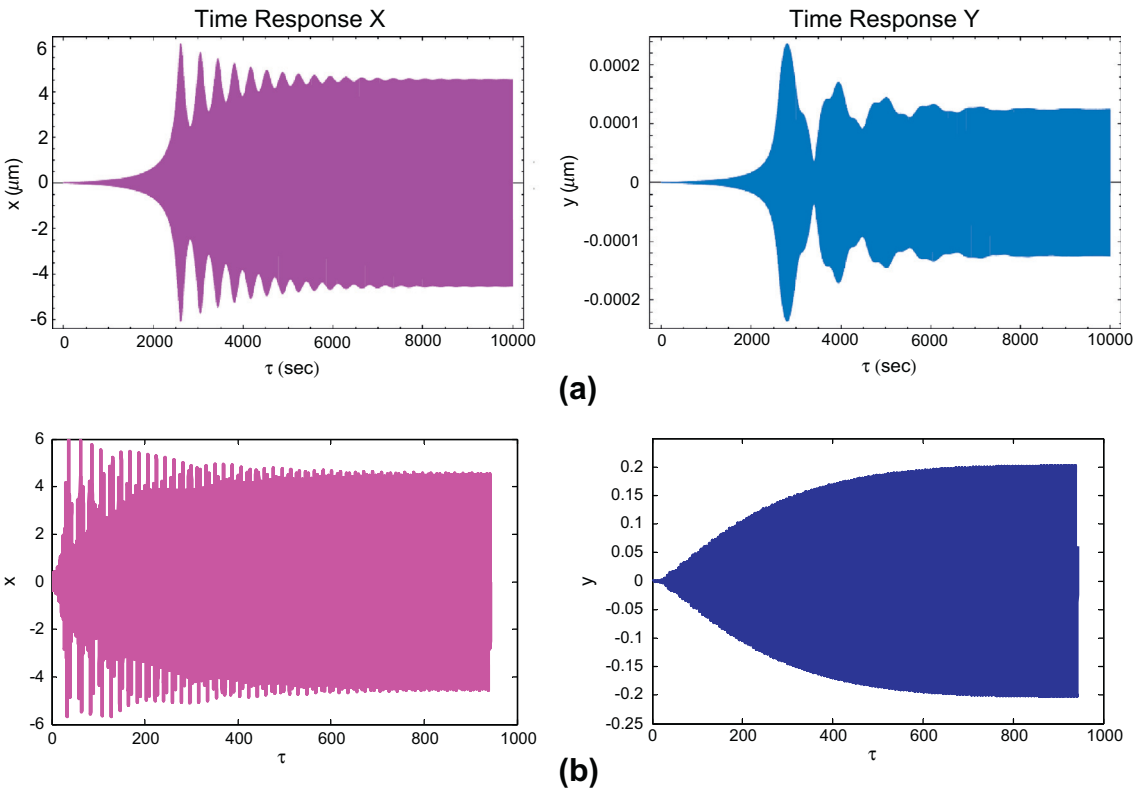

Fig. 9. The dynamic response in the drive mode (left) and the sense mode (right) for (a) the previously reported gyroscope (brought from [22]) and (b) the optimum design reported in this paper.

mismatching. As this figure shows, although the change in amplitude of the drive mode is somehow noticeable, the output of the gyroscope in the sense mode is not changed significantly even for a large difference in stiffness (±10%). This shows the robustness provided by parametric resonance. Note that if harmonic resonance was used instead, even a small difference in the stiffness could reduce the sense mode amplitude to hundredths of the resonance amplitude [1,3].

To sum up the results of this section, the three sets of parameters that contribute to resonance, and consequently to high amplitudes in the sense mode and more accurate readings for the gyroscope, are presented in Table 2. Note that $L^2\delta_{y3} = 1$ was considered and also remember that δ_{x1} and δ_{x3} were related to δ_{y1} and δ_{y3} by Eq. (5).

To illustrate the significant improvement in the output amplitude of the gyroscope with the parameter values lying in the optimum regions found in this study, in Fig. 9 the dynamic response of the previously reported design [15,20–22] is compared to the optimum dynamic performance found here. Fig. 9a is brought from [22] and Fig. 9b is the same as Fig. 6b scaled by L so that it has the same drive amplitude as Fig. 9a. Comparing these two figures, it is clear that the optimum performance found in this paper has an output amplitude as large as large as 1000 times the previously reported design [15,20–22], which makes the reading more accurate in the same order of magnitude (i.e. around 1000 times more accurate). In addition, the response is around 10 times faster in reaching its steady state and, unlike the previously reported design [15,20–22], it has no overshoot in the transient response.

5. Conclusion

This paper provides a parametric study on design of a parametrically excited MEMS gyroscope by studying the effect of each factor on the readings of the sensor. The study shows that although meeting resonance in the parametrically excited drive mode is necessary for having high amplitudes in the sense mode, it is not sufficient and there exist only few distinct sets of parameter values for which resonance-based high amplitude is obtained for the gyroscope. In this paper, three sets of resonance regions for the parametrically excited MEMS gyroscope were obtained. These regions give a dynamic performance approximately 1000 times larger in amplitude and 10 times faster in reaching the steady state, compared to the previous reports for such a device. It was shown here that parametric excitation can provide more accurate readings for a gyroscope and consequently, results in manufacturing of much more accurate gyroscopes.

It was also shown that if parametric resonance is implemented for gyroscopes, even a large difference between the stiffness in the drive and the sense modes due to imperfections in manufacturing, cannot influence the sensor's performance significantly. This property is the most incredible benefit of parametric resonance, because neither

post-manufacturing tunings nor closed loop control methods are able to provide resonance in a gyroscope having a great difference in its modes' natural frequencies.

Appendix A. Deriving the equation of motion

Consider again the structure of the gyroscope illustrated in Fig. 1. To derive the governing equations, we consider the coordinate systems shown in Fig. A1 in which x–y–z coordinate is replaced by x_1–x_2–x_3 system. Note that X_i is the position vector with respect to the fixed Newtonian reference frame, X_i^{brf} is the position vector of the origin of the body reference frame and x_i is the coordinate in the body reference frame. The rotation of the body reference frame is considered to be Ω_i. Using Einstein notation in which a repeating index is equivalent to summation over that index from 1 to 3, the position, velocity and acceleration vectors can be described as in

$$X = X_i^{brf} E_i + x_i e_i \tag{A1}$$

$$\dot{X} = \dot{X}_i^{brf} E_i + \dot{x}_i e_i + \Omega_j E_j \times x_i e_i \tag{A2}$$

$$\ddot{X} = \ddot{X}_i^{brf} E_i + \ddot{x}_i e_i + 2\Omega_j E_j \times \dot{x}_i e_i + \dot{\Omega}_j E_j \times x_i e_i + \Omega_k E_k \times (\Omega_j E_j \times \dot{x}_i e_i) \tag{A3}$$

where E_i is the unit vector in X^{ref} coordinate and e_i is the unit vector in x_1–x_2–x_3 system.

It can easily be shown that the relation between the unity vectors can be described as in Eq. (A4) where Q_i's are presented in Eq. (A5) and ϕ_i's are defined as in Fig. A2.

$$E_i = Q_1 Q_2 Q_3 e_i \tag{A4}$$

$$Q_1 = \begin{bmatrix} \cos\phi_1 & -\sin\phi_1 & 0 \\ \sin\phi_1 & \cos\phi_1 & 0 \\ 0 & 0 & 1 \end{bmatrix},$$
$$Q_2 = \begin{bmatrix} 1 & 0 & 0 \\ 0 & \cos\phi_2 & -\sin\phi_2 \\ 0 & \sin\phi_2 & \cos\phi_2 \end{bmatrix},$$
$$Q_3 = \begin{bmatrix} \cos\phi_3 & -\sin\phi_3 & 0 \\ \sin\phi_3 & \cos\phi_3 & 0 \\ 0 & 0 & 1 \end{bmatrix} \tag{A5}$$

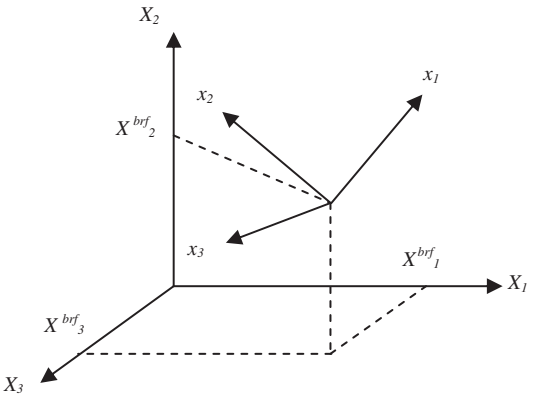

Fig. A1. Coordinate systems for deriving the equation of motion.

Substitution of Eq. (A4) in Eq. (A3) results in

$$\begin{aligned}\ddot{X} = {} & \Big[\ddot{x}_1 + 2\Omega_2\dot{x}_3 - 2\Omega_3\dot{x}_2 + \dot{\Omega}_2 x_3 - \dot{\Omega}_3 x_2 - x_1(\Omega_2^2 + \Omega_3^2) \\ & + x_2\Omega_1\Omega_2 + x_3\Omega_1\Omega_3 + \ddot{X}_1^{brf}(\cos\phi_1\cos\phi_3 \\ & - \sin\phi_1\cos\phi_2\sin\phi_3) + \ddot{X}_2^{brf}(\sin\phi_1\cos\phi_3 \\ & + \cos\phi_1\cos\phi_2\sin\phi_3) + \ddot{X}_3^{brf}\sin\phi_2\sin\phi_3\Big] e_1 \\ & + \Big[\ddot{x}_2 + 2\Omega_3\dot{x}_1 - 2\Omega_1\dot{x}_3 + \dot{\Omega}_3 x_1 - \dot{\Omega}_1 x_3 - x_2(\Omega_1^2 + \Omega_3^2) \\ & + x_1\Omega_1\Omega_2 + x_3\Omega_2\Omega_3 - \ddot{X}_1^{brf}(\sin\phi_1\cos\phi_2\cos\phi_3 \\ & + \cos\phi_1\sin\phi_3) - \ddot{X}_2^{brf}(\sin\phi_1\sin\phi_3 - \cos\phi_1\cos\phi_2\cos\phi_3) \\ & + \ddot{X}_3^{brf}\sin\phi_2\cos\phi_3\Big] e_2 + \Big[\ddot{x}_3 + 2\Omega_1\dot{x}_2 - 2\Omega_2\dot{x}_1 + \dot{\Omega}_1 x_2 \\ & - \dot{\Omega}_2 x_1 - x_3(\Omega_1^2 + \Omega_2^2) + x_1\Omega_1\Omega_3 + x_2\Omega_2\Omega_3 \\ & + \ddot{X}_1^{brf}\sin\phi_1\sin\phi_2 - \ddot{X}_2^{brf}\cos\phi_1\sin\phi_2 + \ddot{X}_3^{brf}\cos\phi_2\Big] e_3 \end{aligned} \tag{A6}$$

Note that the acceleration is presented in the body reference frame in order to simplify the force balance in Newton's second law. External forces in the direction of unit vectors e_i are considered as presented in Eq. (A7), where F^a is the actuation force, F^r is restoring force and F^d is damping force.

$$F_i = F_i^a - F_i^r - F_i^d \tag{A7}$$

Thus, the general form of the equation of motion of the sensor can be derived as Eq. (A8)

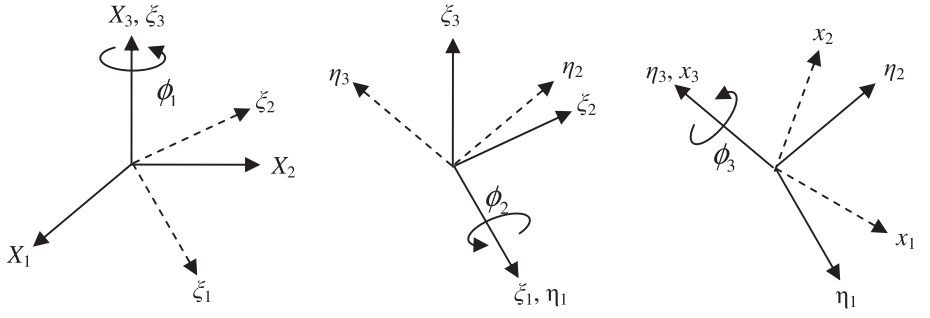

Fig. A2. Definition of describing angles.

$$
\begin{aligned}
m\ddot{x}_1 + F_1^d + F_1^r = F_1^a - m\Big[&2\Omega_2\dot{x}_3 - 2\Omega_3\dot{x}_2 + \dot{\Omega}_2 x_3 - \dot{\Omega}_3 x_2 \\
&- x_1(\Omega_2^2 + \Omega_3^2) + x_2\Omega_1\Omega_2 + x_3\Omega_1\Omega_3 \\
&+ \ddot{X}_1^{brf}(\cos\phi_1\cos\phi_3 - \sin\phi_1\cos\phi_2\sin\phi_3) + \ddot{X}_2^{brf}(\sin\phi_1\cos\phi_3 \\
&+ \cos\phi_1\cos\phi_2\sin\phi_3) + \ddot{X}_3^{brf}\sin\phi_2\sin\phi_3\Big] \\
m\ddot{x}_2 + F_2^d + F_2^r = F_2^a - m\Big[&2\Omega_3\dot{x}_1 - 2\Omega_1\dot{x}_3 + \dot{\Omega}_3 x_1 \\
&- \dot{\Omega}_1 x_3 - x_2(\Omega_1^2 + \Omega_3^2) + x_1\Omega_1\Omega_2 + x_3\Omega_2\Omega_3 \\
&- \ddot{X}_1^{brf}(\sin\phi_1\cos\phi_2\cos\phi_3 + \cos\phi_1\sin\phi_3) - \ddot{X}_2^{brf}(\sin\phi_1\sin\phi_3 - \cos\phi_1\cos\phi_2\cos\phi_3) + \ddot{X}_3^{brf}\sin\phi_2\cos\phi_3\Big] \\
m\ddot{x}_3 + F_3^d + F_3^r = F_3^a - m\Big[&2\Omega_1\dot{x}_2 - 2\Omega_2\dot{x}_1 + \dot{\Omega}_1 x_2 - \dot{\Omega}_2 x_1 - x_3(\Omega_1^2 + \Omega_2^2) + x_1\Omega_1\Omega_3 + x_2\Omega_2\Omega_3 + \\
&\ddot{X}_1^{brf}\sin\phi_1\sin\phi_2 - \ddot{X}_2^{brf}\cos\phi_1\sin\phi_2 + \ddot{X}_3^{brf}\cos\phi_2\Big]
\end{aligned}
\tag{A8}
$$

By considering the following assumptions, Eq. (A9) is obtained.

a. Actuation is applied only in the direction of e_1.
b. The frame has a negligible acceleration, i.e. $\ddot{X}_i^{brf} = 0$.
c. Frame's rotation rate is constant, thus $\dot{\Omega}_i = 0$.
d. Rotation is only in the direction of e_3 i.e. $\Omega_1 = \Omega_2 = 0$.
e. Motion in the direction of e_3 is restricted by comparatively higher stiffness resulting in $x_3 = \dot{x}_3 = \ddot{x}_3 = 0$.

$$
\begin{cases}
m\ddot{x}_1 + F_1^d + F_1^r = F_1^a + 2m\Omega_3\dot{x}_2 + mx_1\Omega_3^2 \\
m\ddot{x}_2 + F_2^d + F_2^r = -2m\Omega_3\dot{x}_1 + mx_2\Omega_3^2
\end{cases}
\tag{A9}
$$

Also, by considering the following assumptions, Eq. (A10) can be obtained which is the same as Eq. (1) in the paper.

f. Dissipation is considered to behave as a viscous damping (linear behavior).
g. Cross-coupling stiffness and damping are neglected, i.e. $F_1^r(x_1, x_2) = F_1^r(x_1)$, etc. and also $F_1^d(x_1, x_2) = F_1^d(x_1)$, etc.
h. Stiffness is considered to act cubically as $F_i^r(x_i) = k_1 x_i + k_3 x_i^3$

$$
\begin{cases}
m\ddot{x}_1 + c_{x_1}\dot{x}_1 + k_1 x_1 + k_3 x_1^3 = F^a + 2m\Omega_3\dot{x}_2 + mx_1\Omega_3^2 \\
m\ddot{x}_2 + c_{x_2}\dot{x}_2 + k_1 x_2 + k_3 x_2^3 = -2m\Omega_3\dot{x}_1 + mx_2\Omega_3^2
\end{cases}
\tag{A10}
$$

References

[1] N. Yazdi, F. Ayazi, K. Najafi, Micromachined inertial sensors, Proceedings of the IEEE 86 (8) (1998) 1640–1658.
[2] S.E. Alper, T. Akin, A symmetric surface micromachined gyroscope with decoupled oscillation modes, in: Proceedings of the 11th International Conference on Solid-State Sensors and Actuators, Munich, Germany, 2001, pp. 456–459.
[3] S.E. Alper, T. Akin, Symmetrical and decoupled nickel microgyroscope on insulating substrate, Journal of Sensors and Actuators, A: Physical 115 (2004) 336–350.
[4] S.E. Alper, T. Akin, A single-crystal silicon symmetrical and decoupled MEMS gyroscope on an insulating substrate, Journal of Microelectromechanical Systems 14 (2005) 707–717.
[5] C. Batur, T. Sreeramreddy, Q. Khasawneh, Sliding mode control of a simulated MEMS gyroscope, ISA Transactions 45 (2006) 99–108.
[6] S. Nasiri, 2008, A Critical Review of MEMS Gyroscopes Technology and Commercialization Status. <www.invensense.com/shared/pdf/MEMSGyroComp.pdf>.
[7] J.A. Chiou, Process window of micromachined gyroscopes subjected to vibrational frequencies, Journal of Sensors and Actuators, A: Physical 125 (2006) 519–525.
[8] S. Park, R. Horowitz, C.W. Tan, Dynamics and control of a MEMS angle measuring gyroscope, Journal of Sensors and Actuators, A: Physical 144 (2008) 56–63.
[9] M. Esmaeili, M. Durali, N. Jalili, Ring microgyroscope modeling and performance evaluation, JVC/Journal of Vibration and Control 12 (2006) 537–553.
[10] V. Bhadbhade, N. Jalili, S. Nima Mahmoodi, A novel piezoelectrically actuated flexural/torsional vibrating beam gyroscope, Journal of Sound and Vibration 311 (2008) 1305–1324.
[11] W.O. Davis, A.P. Pisano, On the vibrations of a MEMS gyroscope, in: Proceedings of the 1st International Conference on the Modelling and Simulation of Microsystems, Semiconductors, Sensors and Actuators (MSM98), 1998, pp. 557–562.
[12] M. Esmaeili, M. Durali, N. Jalili, Modeling and vibration analysis of vibrating beam microgyroscopes under longitudinal rotation of the support, in: Proceedings of the 2005 ASME International Mechanical Engineering Congress and Exposition, IMECE 2005, Orlando, FL, 2005, pp. 345–351.
[13] M. Esmaeili, M. Durali, N. Jalili, Dynamic modeling and performance evaluation of a vibrating cantilever beam microgyroscope, in: Proceedings of the DETC2005: ASME International Design Engineering Technical Conferences and Computers and Information in Engineering Conference, Long Beach, CA, 2005, pp. 137–144.
[14] M. Esmaeili, N. Jalili, M. Durali, Dynamic modeling and performance evaluation of a vibrating beam microgyroscope under general support motion, Journal of Sound and Vibration 301 (2007) 146–164.
[15] L.A. Oropeza-Ramos, C.B. Burgner, K.L. Turner, Robust micro-rate sensor actuated by parametric resonance, Journal of Sensors and Actuators A: Physical 152 (2009) 80–87.
[16] G. Liu, A. Wang, T. Jiang, J. Jiao, J.B. Jang, A novel tuning fork vibratory microgyroscope with improved spring beams, in: Proceedings of the 3rd IEEE International Conference on Nano/Micro Engineered and Molecular Systems, NEMS 2008, Sanya, 2008, pp. 257–260.
[17] W.T. Sung, J.Y. Lee, J.G. Lee, T. Kang, Design and fabrication of an automatic mode controlled vibratory gyroscope, in: Proceedings of the 19th IEEE International Conference on Micro Electro Mechanical Systems, Istanbul, 2006, pp. 674–677.
[18] S. Sung, W.T. Sung, C. Kim, S. Yun, Y.J. Lee, On the mode-matched control of MEMS vibratory gyroscope via phase-domain analysis and design, IEEE/ASME Transactions on Mechatronics 14 (2009) 446–455.
[19] B.S. Chang, W.T. Sung, J.G. Lee, K.Y. Lee, S. Sung, Automatic mode matching control loop design and its application to the mode matched MEMS gyroscope, in: Proceedings of the IEEE International Conference on Vehicular Electronics and Safety, ICVES, Beijing, 2007.
[20] N.J. Miller, S.W. Shaw, L.A. Oropeza-Ramos, K.L. Turner, Analysis of a novel MEMS gyroscope actuated by parametric resonance, in: Proceedings of the ENOC 2008, Saint Petersburg, Russia, 2008.
[21] L.A. Oropeza-Ramos, C.B. Burgner, K.L. Turner, Inherently Robust micro gyroscope actuated by parametric resonance, in: Proceedings of the MEMS 2008, Tucson, AZ, 2008, pp. 872–875.

[22] L.A. Oropeza-Ramos, K.L. Turner, Parametric resonance amplification in a MEMGyroscope, in: Proceedings of the Fourth IEEE Conference on Sensors, Irvine, CA, 2005, pp. 660–663.
[23] J.F. Rhoads, S.W. Shaw, K.L. Turner, The nonlinear response of resonant microbeam systems with purely-parametric electrostatic actuation, Journal of Micromechanics and Microengineering 16 (2006) 890–899.
[24] J.F. Rhoads, S.W. Shaw, K.L. Turner, J. Moehlis, B.E. DeMartini, W. Zhang, Generalized parametric resonance in electrostatically actuated microelectromechanical oscillators, Journal of Sound and Vibration 296 (2006) 797–829.
[25] W. Zhang, K.L. Turner, A mass sensor based on parametric resonance, Solid-State Sensor, Actuator and Microsystems Workshop, Hilton Head Island, South Carolina, 2004, pp. 49–52.
[26] W. Zhang, R. Baskaran, K. Turner, Tuning the dynamic behavior of parametric resonance in a micromechanical oscillator, Applied Physics Letters 82 (2003) 130–132.
[27] W. Zhang, R. Baskaran, K.L. Turner, Effect of cubic nonlinearity on auto-parametrically amplified resonant MEMS mass sensor, Sensors and Actuators, A: Physical 102 (2002) 139–150.
[28] W. Zhang, K.L. Turner, Application of parametric resonance amplification in a single-crystal silicon micro-oscillator based mass sensor, Sensors and Actuators, A: Physical 122 (2005) 23–30.
[29] W. Zhang, K.L. Turner, Frequency-tuning for control of parametrically resonant mass sensors, Journal of Vacuum Science and Technology A: Vacuum, Surfaces and Films 23 (2005) 841–845.
[30] M.V. Requa, K.L. Turner, Precise frequency estimation in a microelectromechanical parametric resonator, Applied Physics Letters 90 (2007).
[31] A. Pakniyat, On the Nonlinear Dynamics and Bifurcations in a New Class of MEMS Gyroscopes with Parametric Resonance, M.S. Thesis, School of Mechanical Engineering, Sharif University of Technology, Tehran, Iran, 2010.